Project 013 Microphysical Modeling & Analysis of ACCESS 2 Aviation Exhaust Observations

Stanford University

Project Lead Investigator

Mark Z. Jacobson
Department of Civil and Environmental Engineering
Stanford University
473 Via Ortega, Room 397
Stanford University, Stanford, CA 94305-4020
Tel: 650-723-6386
jacobson@stanford.edu

University Participants

Stanford University

- P.I.(s): Mark Z. Jacobson, Sanjiva K. Lele
- FAA Award Number: 13-C-AJFE-SU-002, 13-C-AJFE-SU-012
- Period of Performance: 10/01/2014 – 9/30/2016

Project Funding Level

$200,000 from FAA funding

Project Overview

As the popularity of and global access to air travel expands, quantifying its impact on climate and air pollution becomes increasingly important. However, the spatial-temporal distribution of aircraft emissions and their byproducts spans many orders of magnitude, as contrail development begins within seconds, but can spread to the kilometer-scale and persist for hours. The wide range of spatial and temporal scales makes it difficult to obtain detailed knowledge of the composition and evolution of emissions from measurements or modeling studies alone. In an attempt to increase understanding, this project simulates the short-term, near- and far-field evolution of aircraft exhaust aerosol and contrail particles and gases with two computer models: GATOR-GCMOM and an LES model. Together, these two models simulate phenomena spanning a spatial range from millimeters to thousands of kilometers. Detailed microphysical processes in the models are validated and improved with field measurements from NASA's ACCESS-2 campaign, so that the models may provide more credible estimates of impacts on climate and atmospheric composition when used at the regional and global scale.

The Alternative Fuel Effects on Contrails and Cruise Emissions (ACCESS-2) field experiment measured a number of aviation exhaust parameters during flight that are useful for studying the chemical and physical evolution of exhaust gases. Ambient and aircraft engine data from ACCESS-2 are used to initialize model simulations and compare results with measured parameters. Model simulations with GATOR-GCMOM simulate the evolution of aerosol and contrail particle size distributions for comparison with data and with Aerodyne model results (obtained in a parallel study). The high fidelity LES simulations are run to develop a deeper understanding of the dynamics of the evolution of contrails and provide parameters for plume spreading and shearing to GATOR-GCMOM. Results are obtained following the analysis of data from six aircraft flights.

Approach

The Alternative Fuel Effects on Contrails and Cruise Emissions (ACCESS-2) field experiment involved 8 flights performed in May 2014, designed to measure the aircraft exhaust composition and contrail characteristics as a NASA DC-8 source

aircraft burned (1) high sulfur JP-8, and (2) a 50/50 blend of low sulfur JP-8 and a HEFA (hydro-processed esters and fatty acids) biofuel produced from camelina plant oil. The flights were in the 10-11 km altitude range, typical of commercial cruise flight conditions. Sampling of contrails was performed in situ in the national air space (NAS) within the first seconds to minutes of exhaust emission. Statistics were gathered on aerosol/ice emission indices (e.g., grams of ice per kg fuel) from flights using the different fuels. Model simulations are initialized with ambient conditions (temperature, pressure, location, and relative humidity) to match those of the ACCESS 2 campaign.

GATOR-GCMOM is a Reynolds-Averaged Navier-Stokes (RANS) model that treats the microphysical evolution of aerosol size and composition within a subgrid contrail plume. The second model used in this study is a large-eddy simulation (LES) model with a detailed three-dimensional dynamical model. Near-field simulations on the order of several seconds are run with both models, while GATOR-GCMOM simulations continue to capture far-field results.

LES Model

Model Description

Variable	Description
$\boldsymbol{u} = u\boldsymbol{i}+v\boldsymbol{j}+w\boldsymbol{k}$	Filtered air velocity vector
p'	Pressure fluctuation
ρ', ρ_0	Density fluctuation, mean ambient density
$\boldsymbol{G}$	Gravitational acceleration vector
v	Kinematic viscosity of air
θ', θ_0	Potential temperature fluctuation, Reference potential temperature

Table 1: Variable names and descriptions

The LES model to be used for this study is CDP-IF2, an incompressible turbulent flow solver, with Boussinesq approximation for buoyancy effects and Euler-Lagrangian treatment for ice-microphysics [Naiman et al., 2011]. Potential temperature and water vapor concentration are treated as Eulerian fields. The model treats the emissions of aerosols, which are tracked for the primary purpose of simulating contrail development. Water vapor deposition on aerosol particle nuclei is based on local supersaturation. The model treats multiple ice crystal-habits [Inamdar et al., 2013]. It has been used for process studies of persistent aircraft contrails [Naiman et al., 2011; Inamdar et al., 2013] and has supported the development of a subgrid-plume model [Naiman et al., 2010, 2011] for use with global circulation models.

The large eddy simulation (LES) model is described in detail by Naiman [2011]. The following description is taken from Naiman [2011], Naiman et al. [2011], and Inamdar et al. [2013, 2014]. The computational domain for the simulations is stationary with respect to the ground, so the computation represents a temporal simulation. Facing the aircraft, the coordinate system is positioned with the x-axis extending from the left wingtip to the right wingtip of the aircraft, the y-axis pointing opposite gravity, and the z-axis pointing opposite the flight direction.

The large eddy simulation solves the incompressible Navier-Stokes equations with a Boussinesq approximation for buoyancy forces,

$$\nabla . \boldsymbol{u} = 0$$

$$\frac{D\boldsymbol{u}}{Dt} = -\frac{\nabla p'}{\rho_0} + \frac{\rho' \boldsymbol{g}}{\rho_0} + \upsilon \nabla^2 \boldsymbol{u} + \nabla . \boldsymbol{\tau}^{sgs}$$

The subgrid scale stress tensor, $\boldsymbol{\tau}^{sgs}$, is modeled. The Boussinesq approximation gives the equation of state,

$$\frac{\rho'}{\rho_0} = -\frac{\theta'}{\theta_0}$$

Coupled scalar transport equations are solved for potential temperature: θ, water vapor density: Y, and a passive scalar: $\boldsymbol{\varphi}$,

$$\frac{D\theta'}{Dt} = -\frac{d\theta_y}{dy}v + \kappa\nabla^2\theta' + \nabla.\boldsymbol{q}^{sgs,\theta} + \omega_T$$
$$\frac{DY}{Dt} = -\frac{dY}{dy}v + D_v\nabla^2 Y' + \nabla.\boldsymbol{q}^{sgs,Y} + \omega_Y$$
$$\frac{D\varphi'}{Dt} = D_v\nabla^2\varphi' + \nabla.\boldsymbol{q}^{sgs,\varphi}$$

where κ is the thermal diffusivity of air and D_v is the diffusivity of water vapor in air. The passive scalar is tracked to mark engine exhaust. Temperature and water vapor density are prescribed to vary linearly with altitude, so the vertical gradients $d\vartheta_v/dy$ and dY_v/dy are constants. The subgrid scale stress tensors, $\mathbf{q}^{sgs}$, are modeled for each scalar variable. The source terms ω_T and ω_Y couple ice microphysics to the vapor phase through mass exchange of water and latent heat release by ice sublimation/deposition. The terms are related, $\rho_0 C_P \omega_T = -\omega_Y L$, where C_p is the specific heat of air and L is the latent heat of sublimation of ice. The source term ω_Y is calculated in the ice microphysics model described below.

The contrail ice in the simulation is modeled using a Lagrangian tracking approach. The exchange of mass between the Eulerian gas phase and the Lagrangian solid phase is modeled as a deposition/sublimation process. In addition to the conservative mass exchange of water vapor and ice, the heat transfer due to latent heat of sublimation is also modeled through an energy source term in the gas phase. The energy released by this process is applied to the gas phase temperature equation; the solid phase is assumed to be in thermal equilibrium with the gas phase; this is a reasonable assumption given insignificant slip and sedimentation up to 20 min. of time. Contrail particles are assumed to be nonvolatile ice nuclei of a prescribed effective radius that are fully activated for ice deposition and are initially coated in ice. The initial growth and activation of ice nuclei from jet emission products is a complex process and is not treated here. Re-growth is allowed, but other processes, such as additional nucleation, coagulation, and conductive heat transfer between the solid and gas phases are not modeled.

The ice deposition and sublimation calculation is based on a diffusional model. Growth rates are calculated based on the water vapor density field interpolated to the particle location and integrated over the time step. The source of water vapor, ω_Y, is the mass of water deposited to each particle distributed over the local volume from which the water vapor is sourced, ΔV,

$$\omega_Y = \frac{1}{\Delta V}\frac{dm_p}{dt} = \frac{1}{\Delta V}2\pi\rho_p r_p \frac{dr_p{}^2}{dt} N_\mathrm{p}$$

where r_p is the effective spherical radius of the non-spherical ice particle (i.e. radius of a spherical particle of the same mass) and N_p is the number of ice particles represented by each computational particle.

The full equations of motion for spherical particles are complex, but can be simplified for the case of small Stokes number. The Stokes number, St = τ_p/t_0, characterizes the ratio of the particle response time, τ_p, to the characteristic flow time scale, t_0. For small Stokes numbers, particles follow the carrier fluid path lines, so their location, $\boldsymbol{x}_p$, can be advanced in time,

$$\frac{d\boldsymbol{x}_p}{dt} = \boldsymbol{u}(\boldsymbol{x}_p, t)$$

This formulation neglects forces on the particles such as drag and gravitational settling, which become more important for larger Stokes numbers. Over the first twenty minutes of simulation time, a posteriori analysis shows that the maximum Stokes number reached was below 2×10^{-4}, well within the regime of small Stokes number. Sub-grid scale velocity fluctuations are also neglected, since the fluid velocity, u, is the LES filtered velocity.

NASA Data Analysis

Data collected by both the DC-8 and the trailing Falcon were provided for measurements made on 8 separate days. The data collected by NASA on these 8 days – May 7th, 8th, 9th, 10th, 22nd, 27th, 29th and 30th – was collated to observe the inter-day variability in ambient conditions. The following filters were applied to the data:

1. Eliminate all incomplete measurements (i.e. those containing NANs, -99s, -999s)
2. Eliminate all measurements below 10 km altitude
3. Eliminate measurements corresponding to a contrail age of less than 1s

As Figures. 1b and 1c suggest, the local pressure and temperature profiles did not vary significantly between the measurement days. The measured ambient super-saturation w.r.t ice, however, is seen to have a large spread, indicating a large variation in RHi along the flight direction. As the LES model simulates the temporal evolution of a contrail in a stationary ambient, and as the contrail evolution is sensitive to RHi, best estimates of RHi values that span the measured contrail conditions are necessary for the 3-D LES simulations. Thus, data points are clustered (shown in Figure 1a) such that points within a cluster are statistically indistinguishable up to 95% confidence – i.e at a given altitude, the pressure, temperature and RHi in these clusters can be considered almost the same with 95% confidence.

Comparison of LES Simulations and NASA Measurements

It is clear from the data that most contrails evaporated rapidly because of subsaturated ambient air, indicated by the low RHi values (<100%) for most clusters. The highest 2 RHi clusters, however, are seen to sustain a contrail for up to a couple of minutes. These correspond to the measurements made on May 27th and 29th, with the longest-lasting contrail on the 29th. Another point of consideration for the LES model is the inclusion of the impact of fuel sulfur content (FSC). It is known that higher FSC affects jet exhaust by significantly increasing the fine size aerosols. Thus, the LES model incorporates the impact of sulfur by modifying the initialization of contrail particles to include additional fine-size particles. It is observed that the smaller sizes do not impact the integrated quantities of interest, as they do not grow due to inhibition by the Kelvin effect. Kelvin effect refers to the increase in actual vapor pressure due to an increase in curvature of the smaller particles' surface, resulting in preferential evaporation of smaller particles or growth of larger particles.

Finally, in Table 2, we present a comparison of the LES model results and observed data for May 29th. The values of particle concentrations as predicted by the LES are within the margins of error of the observed data. This is promising as it indicates that the LES model is capable of capturing the observed trends in contrail evolution even in subsaturated conditions.

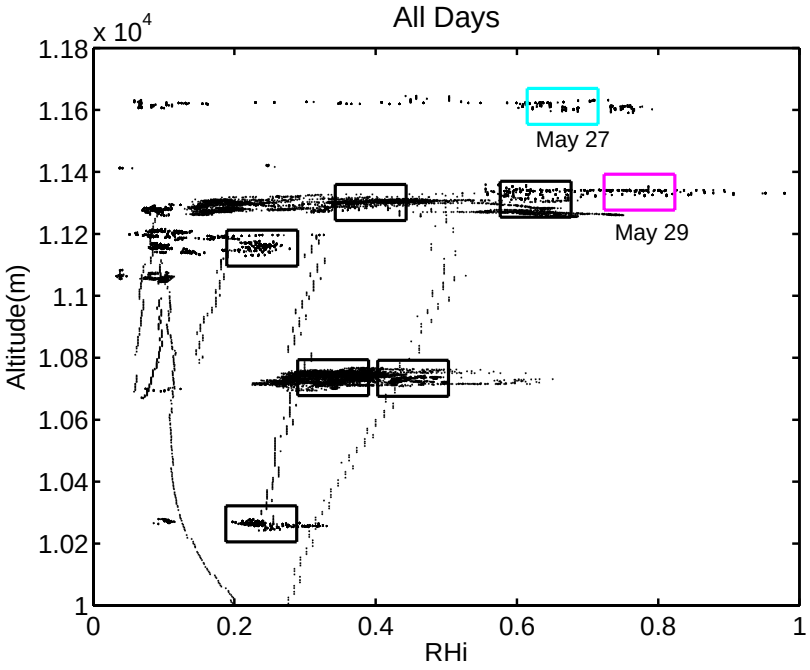

(a)

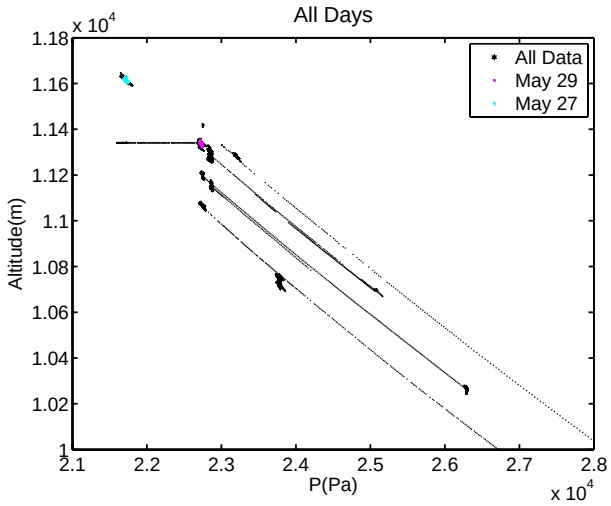

(b)

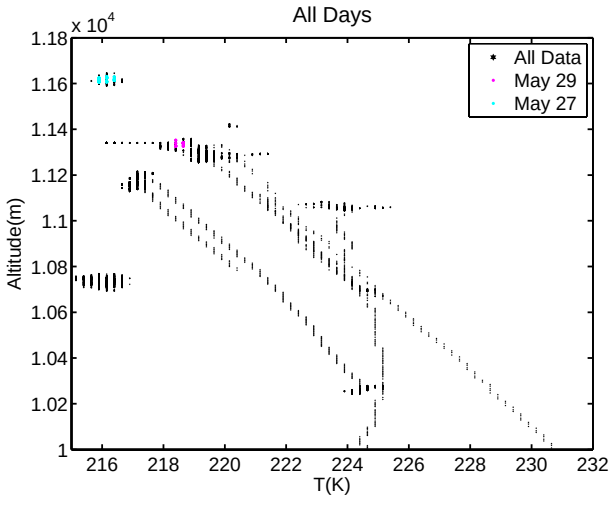

(c)

Figure 1: Analysis of Collated Observational Data: a) Altitude (m) vs. RHi (%); b) Altitude vs. Pressure (Pa); and c) Altitude vs. Temperature (K).

Temperature	Pressure	Stratification	RHi
218 K	227 hPa	-7.2 K/km	77.30%
	Contrail Age (s)	Particle Conc. (#/cm^3)	
		NASA Data	LES Data
	30	53.15 ± 19.53	41.37
	130	25.23 ± 6.3	19.03

Table 2: Comparison of bulk LES results with Data for May 29th

Discrepancies between different LES models

Numerically observed sensitivities of particle survival rates, mean size and mean optical extinction to parameters such as EI_{soot} and ice supersaturation(RHi) reported in the literature [Picot et al., 2015; Unterstrasser, 2014; Naiman et al., 2011] have discrepancies that can be large. Unterstrasser [2014] observes 40% to 70% survival rates for RHi ranging from 120% to 140% and 50% to 90% survival rates for a reduction in EI_{soot} by a factor of 10. In Picot et al. [2015] a change in RHi from 110% to 130% increases survival rate from 65% to near 100% while Naiman et al. [2011] see negligible sensitivity of survival rates to RHi ranging from 110% to 130% and an increase of survival rate from 20% to 90% due to a decrease in EI_{soot} by a factor of 10. In Inamdar et al. [2013] and Lewellen et al. [2014], neglecting the Kelvin effect has a dramatic order-of-magnitude impact on particle survival rates for both young and aged contrails.

We address the important question of whether the observed discrepancies are due to modeling assumptions and differences in simulation initializations. In particular, we examine the impact of changing the Kelvin correction factor that raises the apparent vapor saturation pressure over a curved ice surface relative to a flat one, for a given temperature, T , as follows:

$$p_{sat}^{kelvin} = p_{sat}^{0} \exp\left(\frac{a_k}{r_p}\right) \quad | \quad a_k = \frac{2\sigma M_{H2O}}{RT\rho_p}$$

where r_p is the radius of curvature of the surface, σ is the ice-vapor surface tension, M_{H_2O} is the molecular mass of water, R is the universal gas constant, and ρ_p is the density of ice.

Exclusion of jet exhaust enthalpy is a common modeling assumption [Unterstrasser, 2014] as it is expected to not have any persistent impact. Keeping in mind that several in-situ measurements provide data for young contrails and that Unterstrasser [2014] observes a delayed onset of particle loss as compared to Naiman et al. [2011] and Inamdar et al. [2013], it is necessary to examine the impact of this assumption on the LES of young contrails.
The following cases were run to address the above mentioned issues:

Cases	Description	Legend
B0	$EI_{soot} = 10^{15}$, RHi = 130%, a_k = f(T)	solid black
B1	$EI_{soot} = 10^{15}$, RHi = 110%, a_k = f(T)	dashed black
B2	$EI_{soot} = 10^{15}$, RHi = 130%, $a_k = 10^{-9}$m	solid blue
B3	$EI_{soot} = 10^{15}$, RHi = 110%, $a_k = 10^{-9}$m	dashed blue
B4	$EI_{soot} = 10^{15}$, RHi = 130%, a_k = 0 m	solid red
B5	$EI_{soot} = 10^{15}$, RHi = 110%, a_k = 0m	dashed red

L0	$EI_{soot} = 10^{14}$, RHi = 130%, $a_k = f(T)$	solid green
L1	$EI_{soot} = 10^{14}$, RHi = 110%, $a_k = f(T)$	dashed green
L2	$EI_{soot} = 10^{14}$, RHi = 130%, $a_k = 10^{-9}$m	solid cyan
L3	$EI_{soot} = 10^{14}$, RHi = 110%, $a_k = 10^{-9}$m	dashed cyan
U0	Same as B0, but no jet exhaust enthalpy	solid magenta
U1	Same as B1, but no jet exhaust enthalpy	dashed magenta

Table 3: LES cases for sensitivity to Kelvin Effect

We observe that the cases with low EI_{soot} are indifferent to the Kelvin effect as lower EI_{soot} results in larger ice particles at our simulation initialization and the Kelvin correction affects smaller particles (typically < 0.1 μm). In Fig. 2 we have shown the particle survival rate and mean optical depth for cases with high EI_{soot}.

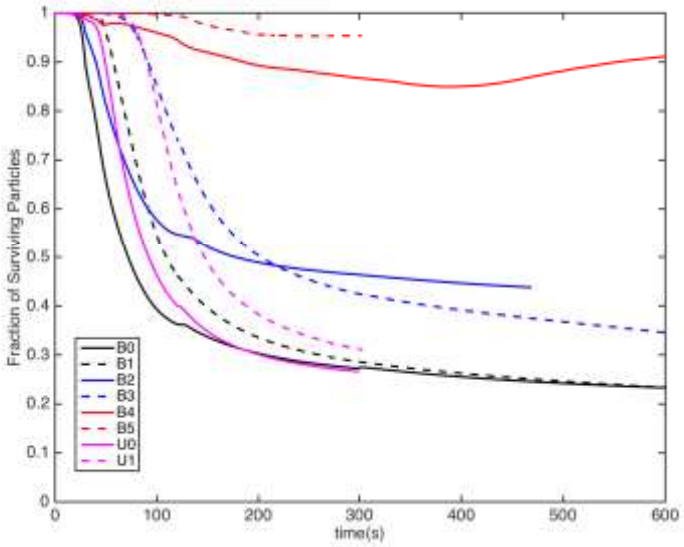

a)

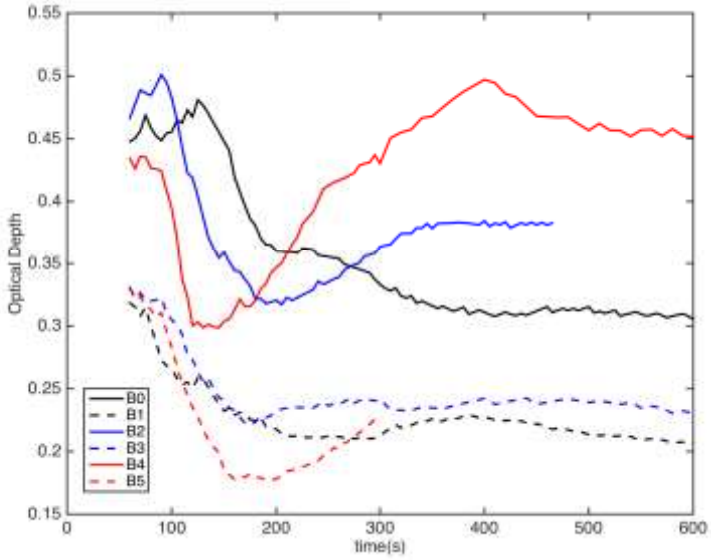

b)

Figure 2: (a) Particle Survival Rate (b) Mean Optical Depth

We can thus conclude the following:

1. The discrepancies in particle survival rates and sensitivities to RHi observed in LES of early contrails using different modeling approaches are primarily due to the different treatment of the Kelvin effect.
2. Particle survival rate and optical depth are the most sensitive to the treatment of the Kelvin effect for high EI_{soot}. This sensitivity is reduced to negligible by lowering the EI_{soot} by a factor of 10.

These results have been submitted to *Atmospheric Chemistry and Physics* [Inamdar et al., 2016, in review]. Results from all LES simulations performed so far are being compiled into a two-part paper [Inamdar et. al., 2016 (b,c)]. As a step towards this, our efforts at developing a reduced order ODE model for contrails up to the vortex phase has been presented [Inamdar et. al., 2016a] at this year's AIAA conference.

GATOR-GCMOM Simulations

GATOR-GCMOM is a one-way nested, online gas-aerosol transport, radiation, general-circulation, mesoscale, and ocean model [Jacobson et al., 2011, 2012, 2013; Whitt et al., 2011]. It is a RANS model that treats gas photochemistry, spectral radiative transfer, size- and composition-resolved aerosol and cloud microphysics and chemistry, dynamical meteorology, and ocean and soil processes. Gas, aerosol, meteorological, and radiative parameters have been evaluated against SCAQS, SARMAP, AERONET, IMPROVE, U.S. EPA monitoring, CARB monitoring, OMI satellite, MODIS satellite, AIRS satellite, and other data.

With respect to aircraft, GATOR-GCMOM treats the subgrid evolution of aircraft exhaust from individual flights with an analytical subgrid plume model (SPM) [Naiman et al., 2010, 2011; Cameron et al., 2013] coupled with a size-and-composition-resolved aerosol and contrail module [Jacobson et al., 2011]. The model also treats subgrid gas chemistry. Emissions from individual flights worldwide are obtained from the 2006 chorded Volpe emission inventory [Wilkerson et al., 2010].

GATOR-GCMOM model simulations are initialized by adding aircraft emissions to a subgrid-scale plume that expands over time, gradually entraining ambient air. Emissions include black carbon (BC), primary organic matter (POM), and sulfate [S (VI)] particulate matter, as well as gaseous water vapor (H_20), CO, CO_2, speciated total hydrocarbons (THCs), NO_x, and SO_2.

Figure 3 shows the change in plume volume due to ambient wind shear and diffusion. At each 1-second time step, coagulation, condensation/evaporation, deposition/sublimation, plume expansion, and contrail dilution is solved as in Jacobson et al. [2011]. To more closely match ACCESS 2 measurements, the baseline scenario is run with parameters given in Table 4. The sensitivity of contrail ice and aerosol size distribution to changes in ambient relative humidity, fuel sulfur content, and black carbon emission index is explored below.

Table 4: Baseline scenario parameters for GATOR-GCMOM

Temperature	216.65 K	**Time Step**	1 second
Pressure	218.4 hPa	**# Vertical layers**	89
Altitude	10.7 km	**# Aerosol size bins**	100
RH-liquid, RH-ice*,+	45%, 76.9%	**Initial plume x-section**	7.5 m x 7.5 m
Fuel sulfur content*	600 ppmm		
BC emissions Factor*	0.03 g-BC/kg-fuel		

*Varied in sensitivity scenarios; + RH-liq=40% for Figures 12-14

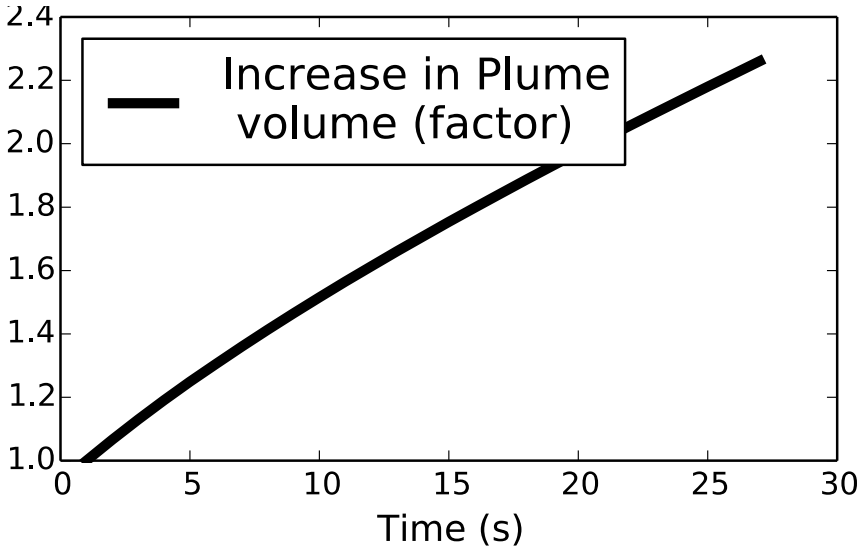

Figure 3: Change in plume volume over the lifetime of the 30-s simulation using GATOR-GCMOM

Baseline Scenario Results

Conditions for the baseline scenario yield aerosol size distributions shown in Figure 4. The contrail aerosols are initialized with a fossil fuel combustion aerosol size distribution shown in yellow ("t=0s") in Figure 4. After the first time step, particles with diameter ~0.03 to 0.2 μm coagulate to form larger particles, which then compete with smaller aerosols for available water vapor. After ~6 seconds, the uptake of all excess water vapor is complete, and RHi within the plume decreases such that evaporation begins (RHi < 100%). Figure 5 shows the change in contrail ice mass concentration as the

entrainment of dry, ambient air outweighs the addition of vapor from exhaust. After 30 seconds, the in-plume ice concentration continues to decrease due to the low ambient relative humidity. The Kelvin effect, a result of surface tension on aerosols that increases the saturation vapor pressure over a curved surface relative to a flat surface, is displayed in Figure 4. The Kelvin effect allows water to evaporate more easily from smaller particles than larger particles. As a result, the smallest particles do not grow, and the largest particles scavenge water from the mid-size particles. After 30 seconds, the number concentration is bimodal, with peaks near 0.01 and ~1 μm.

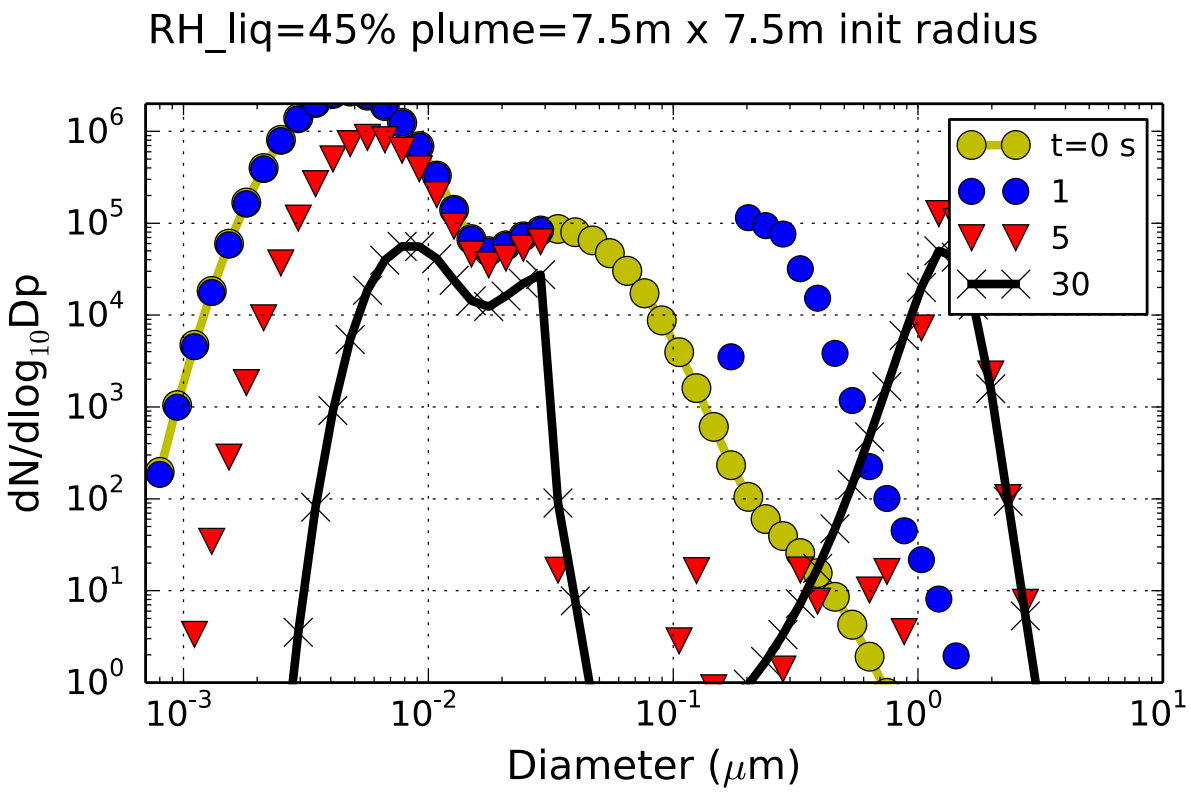

Figure 4: The base case aerosol size distribution (N = #/cm^3) at initialization (0 s) and after 1, 5, and 30 seconds using GATOR-GCMOM. Aerosol composition includes black carbon (BC), primary organic matter (POM), sulfate [S (VI)], and water vapor (H_20).

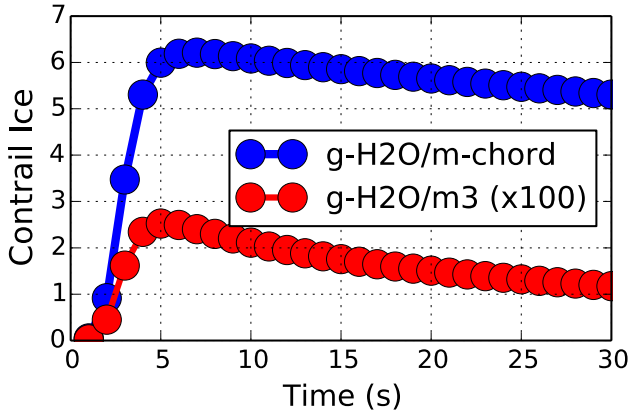

Figure 5: Change in contrail ice concentration (red: g/m^3) and ice concentration per meter of plume chord length (blue, g/m) using GATOR-GCMOM. Values in red are multiplied by 100 for scale.

Sensitivity to Relative Humidity

Figures 6 and 7 show the aerosol size distributions for simulations that vary ambient relative humidity on a logarithmic (left) and linear (right) scale after 23 simulation seconds. As in the baseline case, there is a decrease in small particles from coagulation after initialization, and a decrease in particles around ~0.1 μm from the Kelvin effect. As expected, simulations with relative humidity below the baseline value of 45% show a more rapid loss of ice content, while simulations with higher humidity demonstrate more ice content (Figure 7). Beyond ~60% RH-liquid, volatile particles become saturated and there is no discernible difference from increasing humidity, shown by the overlapping yellow, orange, and red lines.

Sensitivity to Black Carbon Emissions

Figures 8 and 9 show the effects of black carbon emission indices on contrail development. A baseline value of 0.03 g-BC/kg-fuel ("100% Base" case) is representative of Jet-A fuel and the 50% value corresponds to a 50/50 Jet-A/HEFA biofuel blend. The results show that BC has a noticeable effect on the contrail size distributions, but does not significantly affect total ice content after several seconds. In general, a higher BC EI resulted in fewer smaller aerosols, an increase in larger aerosols, and a slight increase in contrail ice.

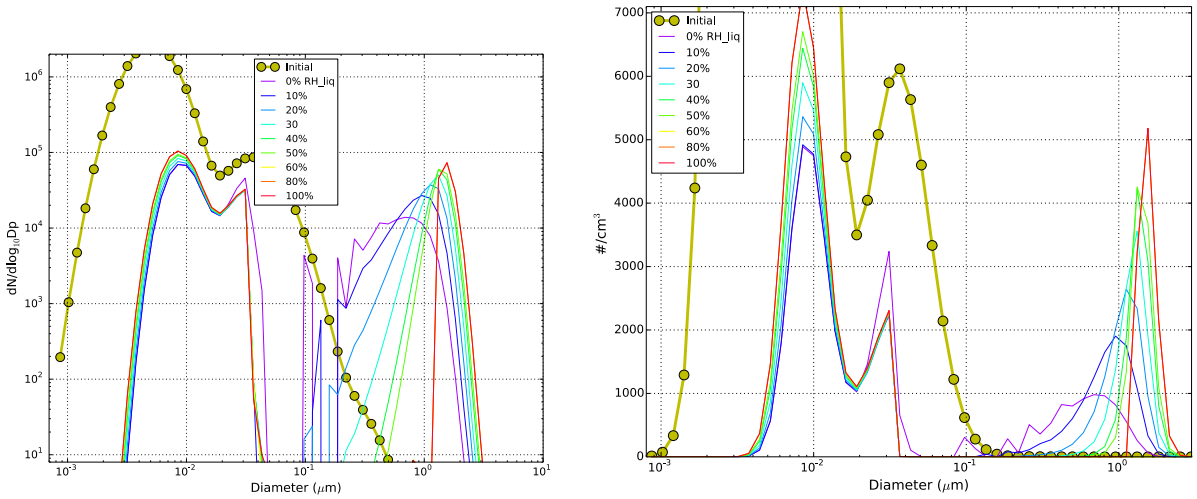

Figure 6: Aerosol size distribution after 23 seconds for simulations with varying ambient relative humidity (RH-liquid) using GATOR-GCMOM. Number concentration (N = #/cm^3) is normalized by size bin diameter (Dp) in the left figure.

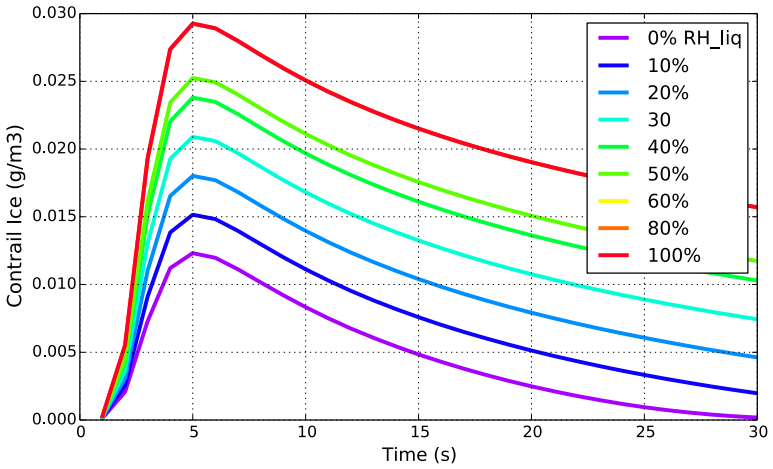

Figure 7: Contrail ice concentration for simulations that vary ambient relative humidity w.r.t. liquid using GATOR-GCMOM. Above 60% RH-liq, activated aerosols are saturated and additional increases in RH do not increase total ice content, shown by overlapping yellow, orange, and red lines.

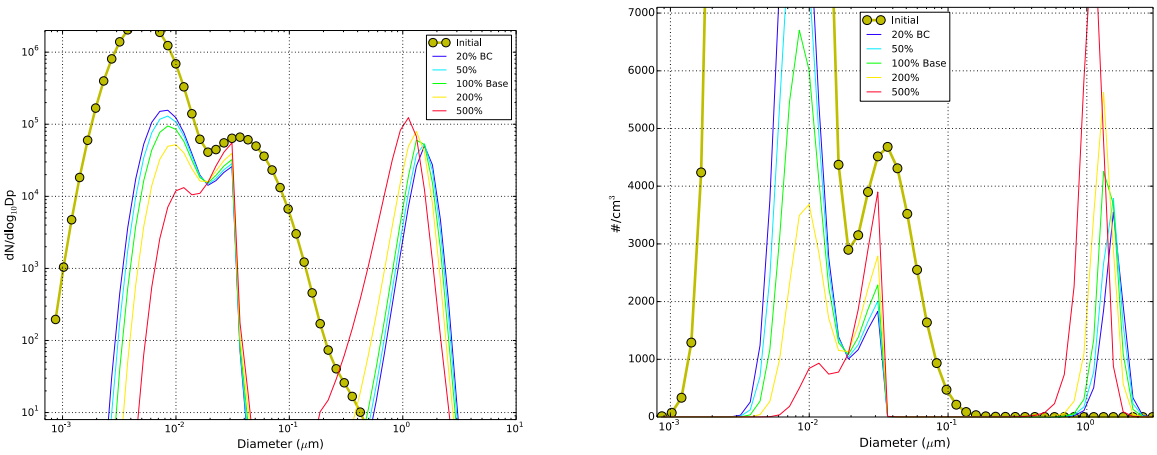

Figure 8: Aerosol size distribution after 23 seconds for simulations using GATOR-GCMOM that vary the BC emission index. Number concentration (#/cm^3) is normalized by size bin diameter (Dp) in the left figure.

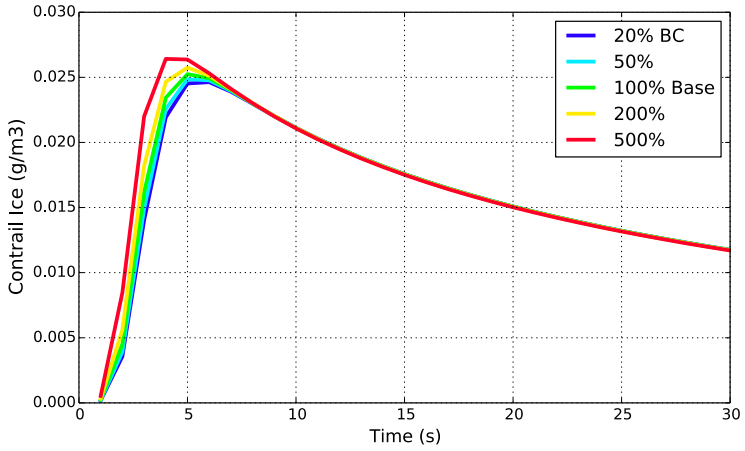

Figure 9: Contrail ice concentration for simulations using GATOR-GCMOM that vary the BC emissions index. An increase in BC results in more initial contrail ice, but the differences diminish after a few seconds.

Sensitivity to Fuel Sulfur Content

Figures 10 and 11 demonstrate the effects of fuel sulfur content (FSC) on aerosol size distribution and ice content after 23 seconds. As with the BC simulation, an increase in FSC showed an initial slight increase in ice content, a decrease in the number concentration of very small aerosols, and an increase in the number of larger aerosols. The baseline FSC is 600 ppmm. A 50/50 Jet-A/HEFA blend has a FSC ranging from ~10-20 ppmm, corresponding to the purple and blue lines in the figures below.

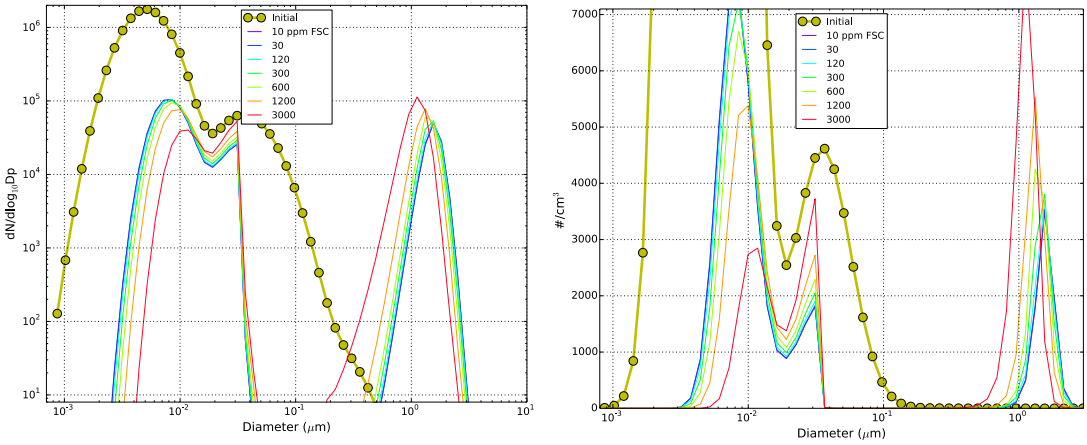

Figure 10: Aerosol size distribution after 23 seconds for simulations using GATOR-GCMOM that vary the fuel sulfur content. Number concentration (#/cm^3) is normalized by size bin in the left figure. The base case uses a FSC of 600 ppmm.

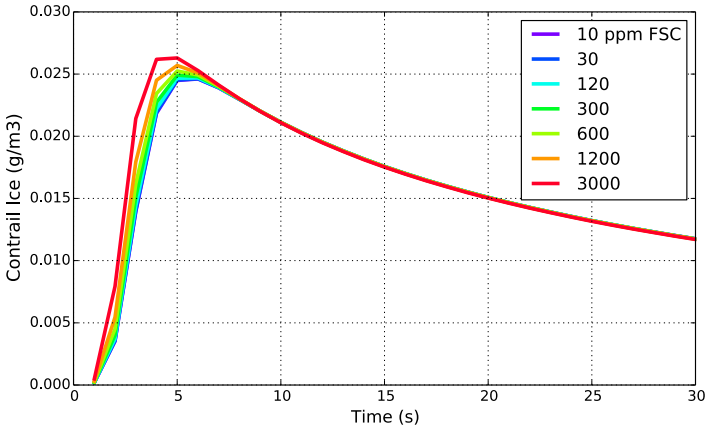

Figure 3: Contrail ice concentration for simulations using GATOR-GCMOM that vary the fuel sulfur content (ppmm). An increase in FSC results in more initial contrail ice, but the differences diminish with time.

Comparison of Model Results with Measurements

Figure 12 shows a comparison of the baseline scenario with contrail measurements taken from the ACCESS 2 campaign on May 29, 2014. This flight was chosen for analysis as it had the longest-lasting contrail, with plume measurements of up to 2 minutes. The size distributions, extracted from 4 instruments (CAS: Cloud and aerosol spectrometer, CIP: Cloud imaging probe, CDP: cloud droplet probe, and UHSAS: Ultra-High Sensitivity Aerosol Spectrometer) are filtered such that all missing data is removed and measurements were taken above 9km altitude. Furthermore, at different time segments, different instruments were directly in the exhaust, and so measurements for the other instruments were discarded. Finally, to further filter ambient data, only data that met at least 1 of the following 3 criteria were used: CO > 117 ppbv, $CO_{2,a}$ > 400 ppmv, and $CO_{2,b}$ > 420 ppmv, where $CO_{2,a}$ is the carbon dioxide mixing ratio taken from the Los Gatos CRD instrument, and $CO_{2,b}$ is the CO_2 mixing ratio measured on the CAS pylon. The age of the plume measurements is determined by the separation distance of the source (DC-8) and chase (NASA HU-25 Falcon) aircraft, and the Mach number of the DC-8. The resulting measurements, separated by age, are shown in the 9 panels of Figure 12. The baseline model size distributions at t=0, 1, 5, 10, 30, 60, 90, 120, 150, and 180 seconds are also shown in panels with data of the same age. For this GATOR-GCMOM simulations, relative humidity (liquid) is 40%.

As shown in Figure 12, the GATOR-GCMOM normalized number concentrations peak at aerosol diameters of 0.01, 0.03, and 1 micron after ~60 seconds. The threshold for the lowest measurable aerosol diameter (UHSAS instrument) is .06 microns, so the smaller GATOR-GCMOM peaks are undetectable. The CAS and CDP probes, however, both show peak number concentrations for aerosols ~1 micron in diameter, with those peak number concentrations close to the modeled GATOR-GCMOM peaks. The maximum CDP number concentrations near ~1um and GATOR-GCMOM results align quite well after 60 seconds (panels 6-9).

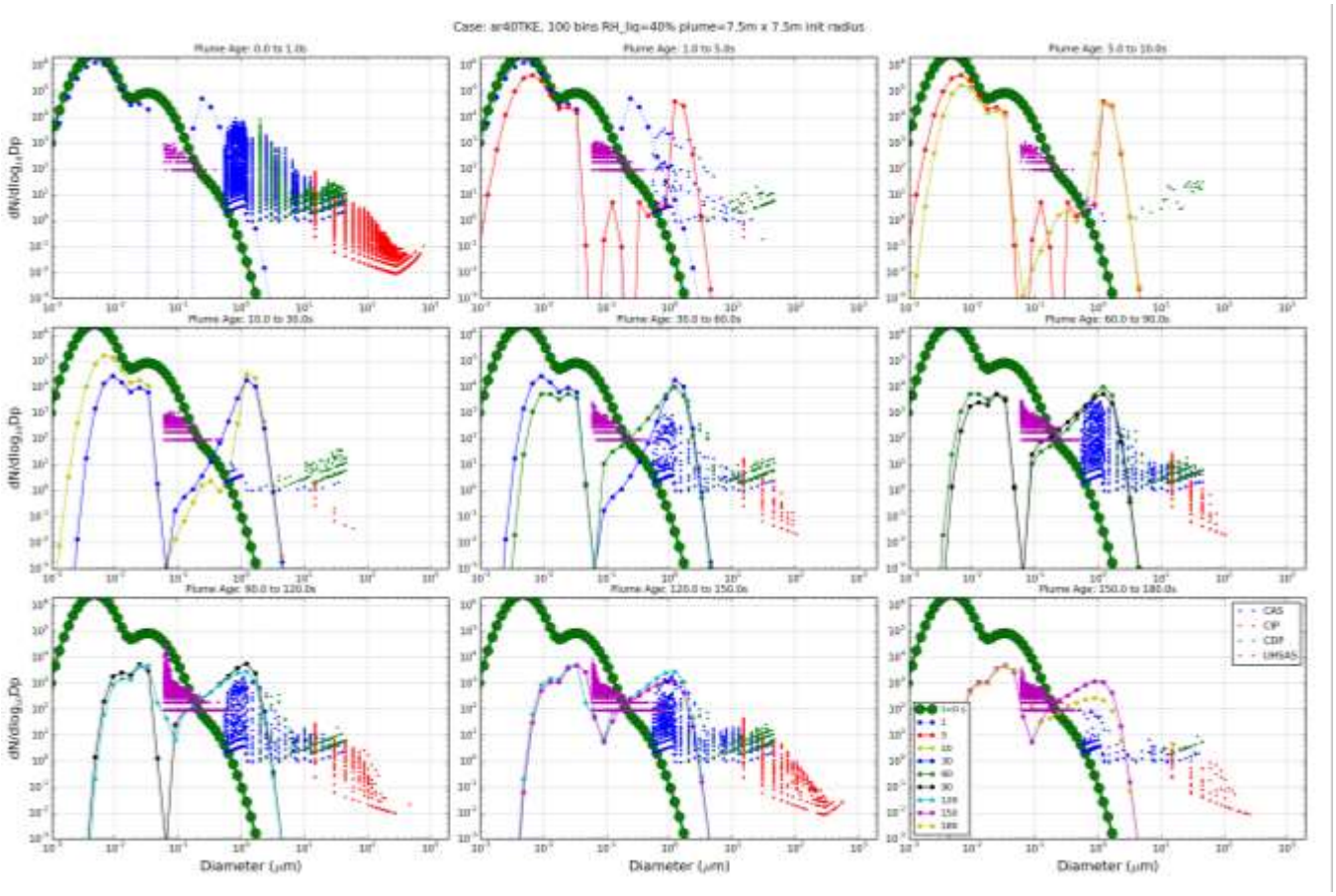

Figure 4: Measured contrail size distributions for the May 29, 2014 ACCESS 2 flight, filtered and separated by plume age. GATOR-GCMOM model results at t=0, 1, 5, 10, 30, 60, 90, 120, 150, and 180s are also shown in panels with data of the same age.

Comparison of GATOR-GCMOM and Aerodyne model results

Figures 13 and 14 show a comparison of model results from the baseline GATOR-GCMOM simulations at 40% (Fig. 13) and 80% (Fig. 14) ambient relative humidity with the Aerodyne simulations also at 40% and 80% RH. The initial distributions for both models are shown in all panels in green circles (GATOR-GCMOM) and red triangles (Aerodyne). The models have quite different initial size distributions, though both show contrail growth within a few seconds, as exhaust vapor raises the in-plume RHi. Both models show peak contrail sizes at or near 1 micron.

In the sub-saturated 40% RH scenario, the smaller aerosols in GATOR-GCMOM coagulate, reducing the number concentrations for smaller size bins within a few seconds. The Aerodyne model shows little change in the small (<.06 μm) size bins, and while initial in-plume supersaturation causes growth of the larger aerosols, the subsequent dehydration as the plume entrains drier ambient air causes the larger contrail particles to return to their initial size distribution (Figure 13, panel 8.) The GATOR-GCMOM distribution, on the other hand, does not return to the original distribution, despite also showing growth and evaporation from the change in plume relative humidity. This is a result of the coagulation of smaller particles into larger ones, that do not break apart after evaporation and thus maintain the larger distribution (Figure 13, panel 9).

In the super-saturated 80% RH scenario, both models show the growth of larger size bins as water freezes onto exhaust aerosols. Both models show number concentration peaks for larger particles in the 1-4 μm diameter range. Both models

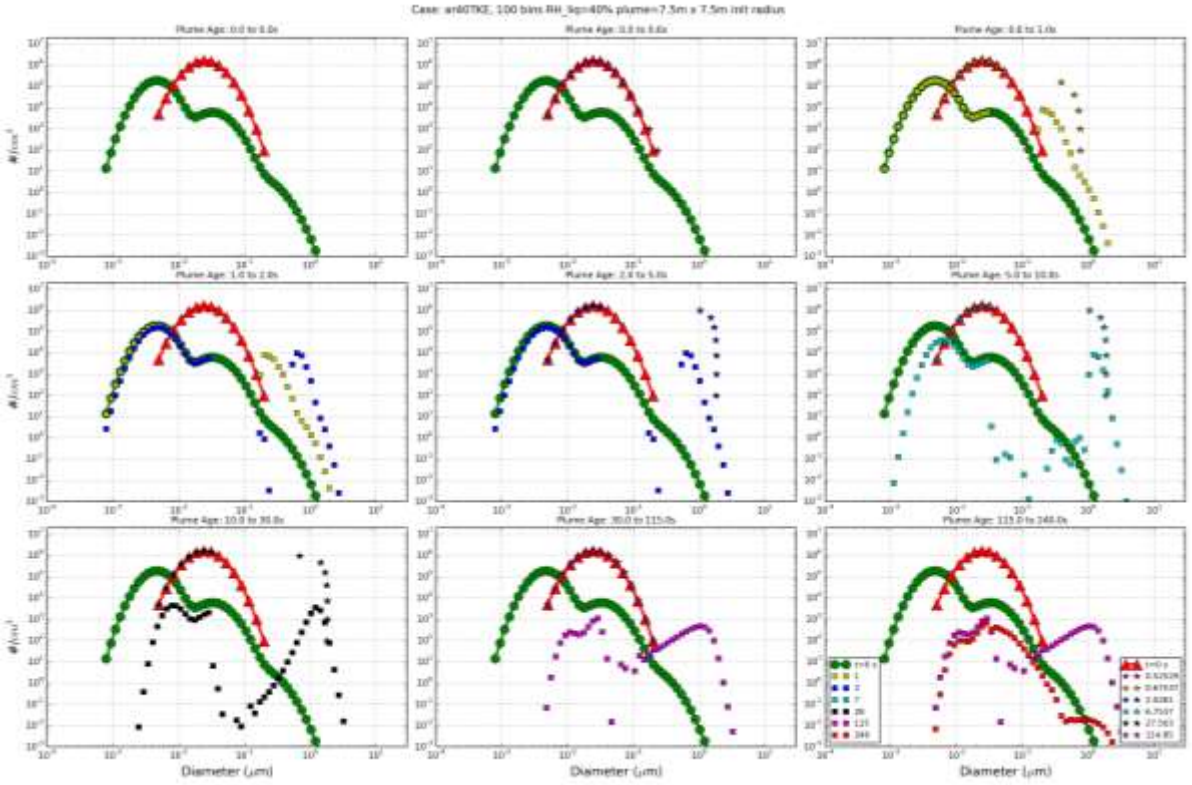

Figure 5: Comparison of GATOR-GCMOM (squares) and Aerodyne (stars) modeled number concentrations (#/cm^3) at 40% ambient relative humidity. Initial distributions for GATOR-GCMOM (green circles) and Aerodyne (red triangles) are also shown in each panel.

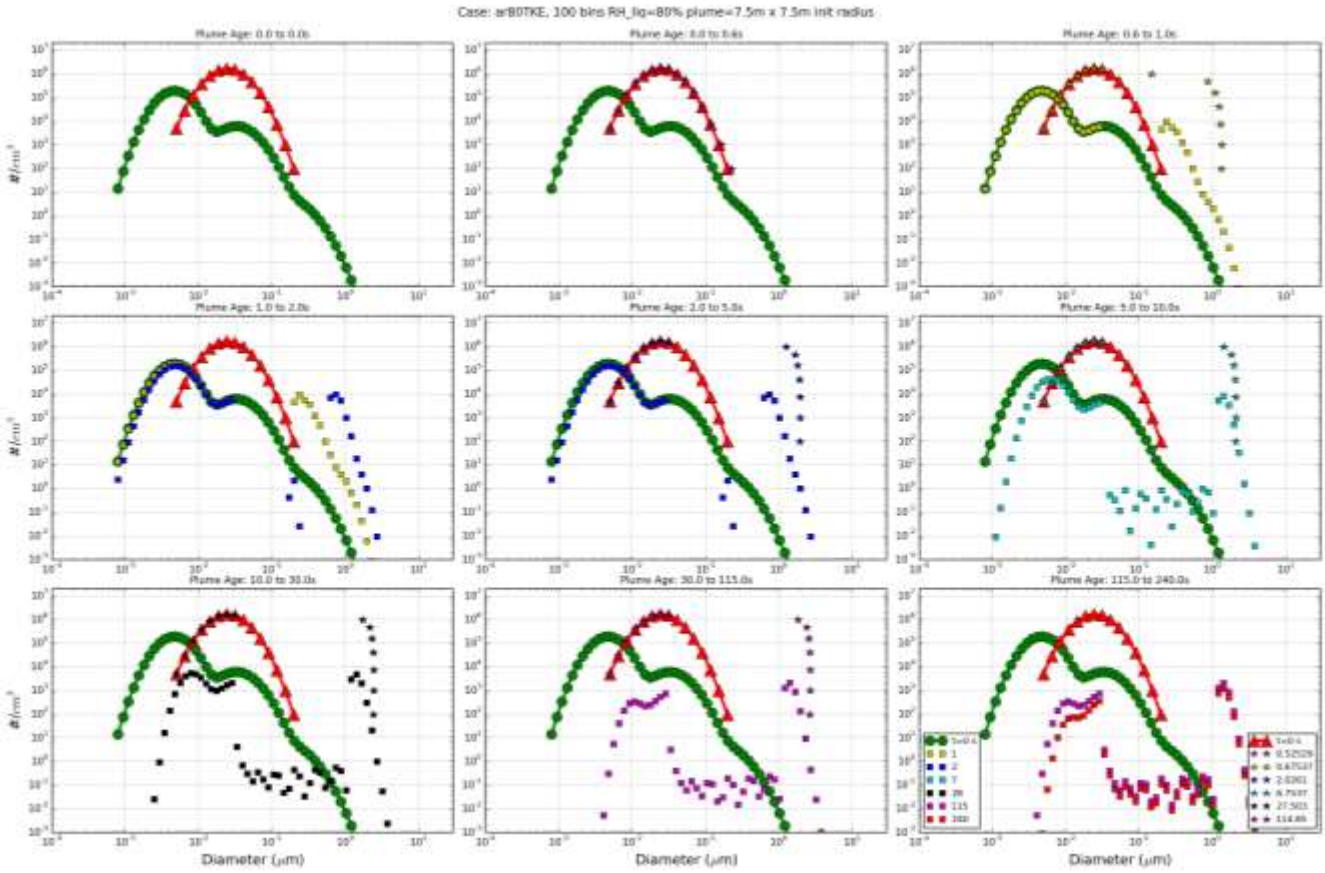

Figure 6: Comparison of GATOR-GCMOM (squares) and Aerodyne (stars) modeled number concentrations (#/cm^3) at 80% ambient relative humidity. Initial distributions for GATOR-GCMOM (green circles) and Aerodyne (red triangles) are also shown in each panel.

Future Research Directions

The present work helps illuminate the effects of alternative aviation fuels on contrail properties. However, additional analysis and comparison with measured data sets are required before firm conclusions on such effects can be made. At present, the available contrail size distribution data shows large measured contrail particles that may not be realistic. As data becomes available, it may be beneficial to reevaluate model results for comparison with more thoroughly filtered contrail measurements, including: (1) volatile and non-volatile aerosol number, mass, and composition, and (2) ice particle number and size. Datasets from partner institutions (DLR and Transport Canada) also involved in ACCESS-II measurement campaign may provide additional measurements from both the ACCESS 2 campaign, as well as the older CONCERT campaign that includes far-field (~10-20 minute) measurements. In particular, the completed 20-minute supersaturated LES and GATOR-GCMOM cases may be compared with the measured aged contrails from the CONCERT campaign for longer-lived contrail modeling.

References

Cameron, M.A., M.Z. Jacobson, A.D. Naiman, and S.K. Lele, Effects of plume-scale versus grid-scale treatment of aircraft exhaust photochemistry, *Geophys. Res. Lett., 40*, 5815-5820, 2013.

Inamdar A.R., Lele S.K., Jacobson M.Z., A Probabilistic Ice Habit Model for LES of Contrails, *5th Atmos. & Space Env. Conference*, AIAA control number 1586391, 2013.

Inamdar A. R., Lele S. K., and Jacobson M. Z., LES of Contrails With Ice Habit Treatment Using the Fickian-Distribution Model. ASME 4th Joint US-European Fluids Engineering Division Summer Meeting, 2014.

Inamdar A. R., Lele S. K., and Jacobson M. Z., Reduced Order Modeling of Contrails: Jet Induction and Vortex Phases, AIAA Conference, 2016a.

Inamdar A. R., Naiman A.D., Lele S. K., and Jacobson M.Z., Sensitivity of Particle Loss to the Kelvin Effect in Young Contrails, Atmospheric Chemistry and Physics Discussions, in review, 2016b.

Inamdar A. R., Naiman A.D., Lele S. K., and Jacobson M.Z., Sensitivity of Early Persistent Contrails to Aircraft Type, Ambient Conditions and Microphysical Modeling, Part I: LES Results, Atmospheric Chemistry and Physics, in progress, 2016b.

Inamdar A. R., Naiman A.D., Lele S. K., and Jacobson M.Z., Sensitivity of Early Persistent Contrails to Aircraft Type, Ambient Conditions and Microphysical Modeling, Part II: ODE Model Results, Atmospheric Chemistry and Physics, in progress, 2016c.

Jacobson, M.Z., J.T. Wilkerson, A.D. Naiman, and S.K. Lele, The effects of aircraft on climate and pollution. Part I: Numerical methods for treating the subgrid evolution of discrete size- and composition-resolved contrails from all commercial flights worldwide, J. Comp. Phys., 230, 5115-5132, doi:10.1016/j.jcp.2011.03.031, 2011, http://www.stanford.edu/group/efmh/jacobson/Articles/VIII/aircraftflights.html.

Jacobson, M.Z., J.T. Wilkerson, S. Balasubramanian, W.W. Cooper, Jr., and N. Mohleji, The effects of rerouting aircraft around the Arctic Circle on Arctic and global climate, *Climatic Change*, 115, 709-724, doi:10.1007/s10584-012-0462-0, 2012.

Jacobson, M.Z., J.T. Wilkerson, A.D. Naiman, and S.K. Lele, The effects of aircraft on climate and pollution. Part II: 20-year impacts of exhaust from all commercial aircraft worldwide treated individually at the subgrid scale, *Faraday Discussions*, *165,* 369-382*,* doi:10.1039/C3FD00034F, 2013, http://www.stanford.edu/group/efmh/jacobson/Articles/VIII/aircraftflights.html.

Lewellen, D.C., Meza, O., and Huebsch, W.W., Persistent Contrails and Contrail Cirrus. Part I: Large-Eddy Simulations from Inception to Demise, Journal of the Atmospheric Sciences, 71, 4399-4419, 2014.

Naiman, A.D., S.K. Lele, J.T. Wilkerson, and M.Z. Jacobson, Parameterization of subgrid aircraft emission plumes for use in large-scale atmospheric simulations, *Atmos. Chem. Phys.*, 10, 2551-2560, 2010.

Naiman, A.D., S.K. Lele, and M.Z. Jacobson, Large eddy simulations of contrail development: Sensitivity to initial and ambient conditions over first twenty minutes, *J. Geophys. Res.*, *116*, D21208, doi:10.1029/2011JD015806, 2011.

Naiman, A.D., Modeling Aircraft Contrails and Emission Plumes for Contrail Impacts, Ph.D. Dissertation, Stanford University, 2011.

Picot, J., Paoli, R., Thouron, O., Cariolle, D., Large-eddy Simulations of Contrail Evolution in the Vortex Phase and its Interaction with Atmospheric Turbulence, Atmospheric Chemistry and Physics, 15, 7369-7389, 2015.

Unterstrasser, S., Large-eddy Simulation Study of Contrail Microphysics and Geometry During the Vortex Phase and Consequences on Contrail-to-Cirrus Transition, Journal of Geophysical Research: Atmospheres, 119, 7537-7555, 2014.

Whitt, D.B., J.T. Wilkerson, M.Z. Jacobson, A.D. Naiman, and S.K. Lele, Vertical mixing of commercial aviation emissions from cruise altitude to the surface, *Journal of Geophysical Research.*, *116*, D14109, doi:1029/2010JD015532, 2011, www.stanford.edu/group/efmh/jacobson/Articles/VIII/aircraftflights.html.

Wilkerson, J.T., M.Z. Jacobson, A. Malwitz, S. Balasubramanian, R. Wayson, G. Fleming, A.D. Naiman, and S.K. Lele, Analysis of emission data from global commercial aviation: 2004 and 2006, *Atmos. Chem. Phys., 10*, 6391-6408, 2010, www.stanford.edu/group/efmh/jacobson/Articles/VIII/aircraftflights.html.